Comparison of methane detection for shortwave and longwave infrared hyperspectral sensors under varying environmental conditions

Lucy A. Zimmerman[a] and John P. Kerekes[a]

[a]Chester F. Carlson Center for Imaging Science, Rochester Institute of Technology, Rochester, NY

ABSTRACT

Identifying methane gas emissions sources is crucial to the mitigation of greenhouse gas emissions, and hyperspectral imagery is effective at methane leak detection. Hyperspectral sensors in both the shortwave infrared (SWIR) and longwave infrared (LWIR) can detect methane plumes, but surface background and atmospheric conditions cause methane detectability to vary depending on the sensor's spectral region. This study compared methane detectability under varying background conditions for two airborne hyperspectral sensors: AVIRIS-NG in the SWIR, and HyTES in the LWIR. The trade study modeled methane plumes under a wide variety of conditions by making use of synthetic images generated using MODTRAN radiance curves, and applying a matched filter for methane detection. The modeling method was validated through comparison with real AVIRIS-NG and HyTES data. In the SWIR, the factors which most strongly influenced methane detectability were surface reflectance of the background and surface reflectance directly underneath the methane plume. In the LWIR, the temperature of the methane plume and the temperature of the surface had the highest impact on methane detection. We computed the specific boundaries on these conditions which make methane most detectable for each instrument. The results of this trade study can help inform decision making about which sensors are most useful for various methane studies, such as leak detection, plume mapping, and emissions rate quantification.

Keywords: Hyperspectral, methane detection, remote sensing, AVIRIS-NG, HyTES, greenhouse gas

1. MOTIVATION AND BACKGROUND

Greenhouse gas emissions are a pervasive issue; there are a wide variety of sources emitting various heat-trapping gases at accelerating rates, many of which are not accurately monitored and thus cannot be mitigated. Methane is the second most prevalent among these gases, and with heat trapping capabilities of up to 21 times those of carbon dioxide (the most abundant greenhouse gas), it has an outsized effect on climate change.[1] In the United States, an estimated 25%-40% of total methane emissions come from oil and natural gas sector sources.[2,3] In order to reduce methane emissions, these emission sources must be identified and located; however, with the EPA's inventory of greenhouse gas emissions estimated to be a factor of 1.7 too low, gas emissions monitoring still requires development in order to be comprehensive and actionable.[2]

Hyperspectral imagery, using both the shortwave and longwave infrared regions, can effectively detect methane point source emissions. Airborne hyperspectral sensors have the capability to detect high concentrations of methane emitted from a small area, to include the majority of emissions from the fossil fuel industry. Two of these airborne sensors which have both detected methane and quantified methane plume concentrations are AVIRIS-NG in the SWIR and HyTES in the LWIR.[4–7] AVIRIS-NG covers a wavelength range of 0.35-2.51 μm, encompassing both methane absorption bands in the SWIR, and has 5 nm spectral resolution. HyTES covers a spectral range of 7.5- 12.0 μm with approximately 17 nm spectral resolution. This covers the methane absorption band centered at 7.7 μm.

Methane detection accuracy using various hyperspectral sensors can fluctuate depending on atmospheric and background conditions. AVIRIS-NG has been shown to have high retrieval inaccuracies when the methane plume

Further author information:
L.A.Z.: E-mail: laz1558@rit.edu

is located over water.[8] Methane detecting instruments in the LWIR may be more effective at methane detection when the methane plume is cooler than the surrounding ground and when atmospheric water vapor concentration is low.[9]

This study evaluated the limitations posed by background conditions on methane detection using AVIRIS-NG and HyTES. We assessed the atmospheric and background conditions which have the highest impact on methane detectability for both sensors and evaluated the limits on these conditions which preclude or enhance methane detection. To describe this trade study, we first detail the methods for simulating AVIRIS-NG and HyTES data. We next explain the validation of simulated data with published experimental data, and lastly present the results and conclusions of the study.

2. METHODS

In this study, we evaluated methane detectability for the background conditions which have the highest impact on methane detection for AVIRIS-NG and HyTES: surface temperature, methane plume temperature, surface reflectance, and methane concentration. These conditions can widely vary, so collecting data for a sufficient range of background conditions is not reasonable. Instead, we generated synthetic images to model a variety of background conditions. The process for image generation is comprised of 3 steps for each sensor: (1) generate radiance curves in MODTRAN, (2) assemble the background region of the image, and (3) add sensor noise. Following image generation, a matched filter was applied to the synthetic image, and the area under the ROC curve was used as a performance metric.

2.1 Radiance Curve Generation

In step 1, radiance curves were generated using MODTRAN6, making use of the chemical plume model to produce on-plume radiance curves passing through a methane plume and off-plume radiance curves not passing through the plume.[10] For HyTES, the radiance curve was the at-sensor radiance term, and for AVIRIS-NG, radiance curves were created using MODTRAN direct reflected and path radiance terms.

2.2 Background Image Generation

Step 2 is the generation of a background region for the image. In order to avoid signal contamination when computing the matched filter, the synthetic images contained separate on-plume and off-plume regions. The background covariance was taken over the off-plume region, so this portion of the image must have realistic variation. For AVIRIS-NG, this background variation was created by generating radiance curves for the surface reflectances retrieved from a real scene. These retrieved reflectances were from a simultaneous AVIRIS-NG and HyTES flight over a methane emissions source in the Four Corners region of the United States.[11] The radiance curves at each pixel of the background image were generated using a different reflectance curve, but all other atmospheric inputs were the same across the whole image. Figure 1a shows the radiance of an example AVIRIS-NG synthetic image at a single band. The on-plume region spans a few columns on the left hand side of the image, while the off-plume region makes up the majority of the image and has visible variation. The radiance curves used to create the on-plume region have passed through a methane plume, but the off-plume region contains only ambient atmospheric methane. There is no realistic looking plume structure in these images because the matched filter does not rely on spatial properties of the image; we attempt to model natural variation not for spatial similarity, but to ensure that the covariance of synthetic images is similar to real images.

For HyTES, background variation was created using surface temperature rather than surface reflectance. All radiance curves in the background region of the image were computed using the same atmospheric conditions and surface emissivities, but they represent surface temperatures that vary within 7 K of the on-plume surface temperature. This range of temperatures was based on retrieved surface temperature data from the Four Corners simultaneous overflight.[11] Figure 1b shows an example HyTES synthetic image. The locations of the on- and off-plume regions are the same as the AVIRIS-NG image.

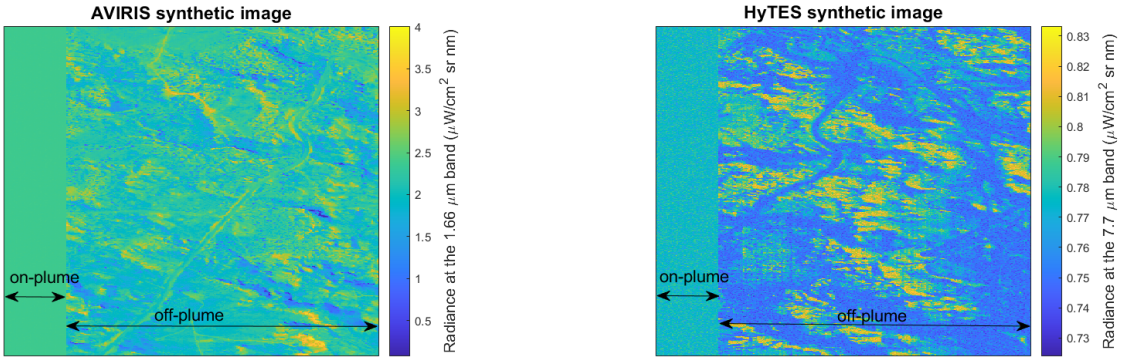

(a) (b)

Figure 1: (a) AVIRIS-NG example synthetic image; radiance shown at the 1.66 μm band. (b) HyTES example synthetic image; radiance shown at the 7.7 μm band.

2.3 Instrument Noise Addition

Step 3 is the addition of realistic instrument noise to the synthetic image based on the Noise Equivalent delta Radiance curve for each sensor. AVIRIS-NG noise was assumed to be signal dependent, so its NEdL curve was calculated using the radiance and the AVIRIS-NG SNR.[12–14] HyTES was assumed to have a constant NEdL curve.[15] To add noise to the images, each band of the NEdL curve was scaled by a random number from $X \sim N(0,1)$. These randomly scaled NEdL curves were calculated for each pixel of the image and were added to the radiance curve at each pixel.[16]

2.4 Matched Filter

A matched filter was used to detect methane in synthetic images. The methane absorption spectrum from the HITRAN database was the target spectrum; for each sensor, the signature was convolved to the sensor response.[17] Pixels that are flagged by the matched filter in the on-plume region of the image are correct detections, and pixels flagged in the off-plume region are false alarms.

3. VALIDATION

In order to ensure that the MODTRAN generated images and the method of evaluating methane detectability was reasonable, the synthetic data was compared with real AVIRIS-NG and HyTES data. First, single MODTRAN generated radiance curves were compared to real AVIRIS-NG and HyTES data, and second, the background variation in full synthetic images was compared to real images. The real data for this validation came from the Four Corners study which was used to add background variation to synthetic images discussed in section 2.2.[11]

3.1 Radiance Curve Validation

The first step in the validation was comparing MODTRAN generated radiance curves with radiance curves in real AVIRIS-NG and HyTES images. We produced radiance curves in MODTRAN using atmospheric and surface conditions that were as close as possible to the true conditions. Our simulated radiance curves were in good agreement with the real radiance curves, as shown in figure 2.

3.2 Synthetic Image Validation

The second step in the validation was to ensure that the background variation in synthetic images was representative of natural variation. To accomplish this, we generated synthetic images for AVIRIS-NG and HyTES using the background conditions present on the day of the Four Corners data collect, and compared the results of the matched filter between real and synthetic images. A visual comparison of the radiance in the real and synthetic

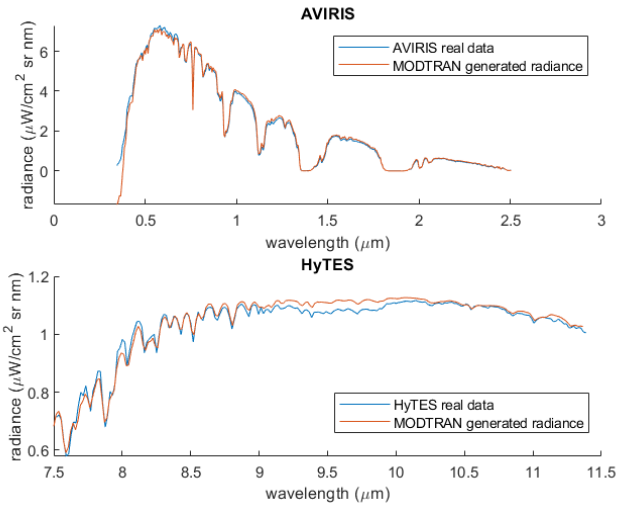

Figure 2: Comparison of MODTRAN generated radiance curves with radiance curves from real AVIRIS-NG and HyTES data

images is shown in figure 3 for AVIRIS-NG and in figure 4 for HyTES. The synthetic image was generated using the same methods outlined in section 2.

After applying a matched filter to the real and synthetic data, the areas under the ROC curves for both real and synthetic images were within less than 1% for AVIRIS-NG and less than 3% for HyTES. This demonstrates that there is good agreement for detection statistics on a real and synthetic image under the same conditions, and shows that the method of creating background variation is realistic.

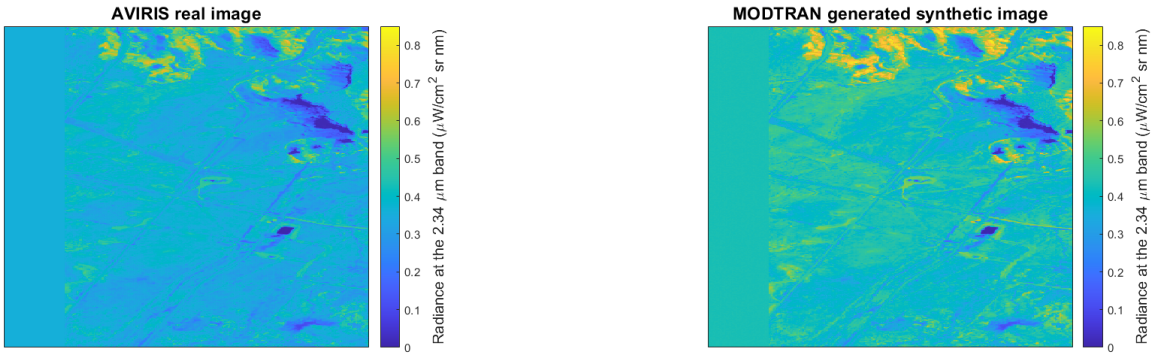

(a) (b)

Figure 3: (a) Radiance at the 2.2 μm band for (a) AVIRIS real validation image and (b) AVIRIS synthetic validation image

4. RESULTS

The accuracy of methane detection for this trade study was evaluated using the area under the ROC curve. In order to understand how background conditions impact AVIRIS-NG and HyTES methane detection capabilities, the areas under the ROC curve were compared for a range of conditions. We use an area under the ROC curve of 0.8 as a threshold for detectability.

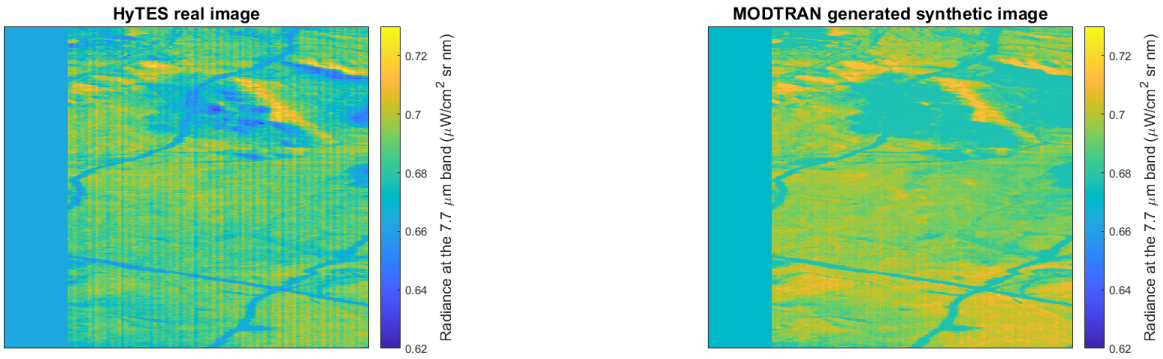

(a) (b)

Figure 4: (a) Radiance at the 7.7 μm band for (a) HyTES real validation image and (b) HyTES synthetic validation image

4.1 AVIRIS-NG results

The two factors which had the highest impact on methane detectability for AVIRIS-NG were plume concentration, and contrast between surface reflectance of the background and surface reflectance below the plume. The surface reflectance of the background region in the image is referred to as the off-plume surface reflectance, and the reflectance of the surface directly below the methane plume is the on-plume surface reflectance. Figure 5a shows a comparison of areas under the ROC curve for varying on-plume and off-plume surface reflectances, with a 500 ppm concentration methane plume. The off-plume surface reflectance on the y-axis is an average over all methane bands over all pixels in the background. This figure shows that the area under the ROC curve was at its highest when the on-plume reflectance was 1.25-1.8 times greater than the off-plume reflectance; in this range, the area under the ROC curve was greater than 0.8, which is a reasonable detection threshold. When the on-plume reflectance was much lower than the off-plume reflectance, the matched filter flagged the methane feature as an emission, and this caused the low areas under the ROC curve shown in blue on the figure. Figure 5b shows the same trend, but with a 2500 ppm concentration methane plume. The higher concentration broadened the area over which methane was highly detectable: for this concentration, methane was highly detectable when on-plume reflectance was 0.6-3.0 times greater than off-plume reflectance. The areas under the ROC curve for a 2500 ppm plume peaked at 0.99, whereas area under the ROC curve for a 500 ppm plume peaked at 0.8. Therefore, methane at a lower concentration was not highly detectable by AVIRIS-NG under any surface reflectance conditions, but at a higher concentration, methane was highly detectable for on- and off- plume reflectance ratios ranging from 0.6-3.0.

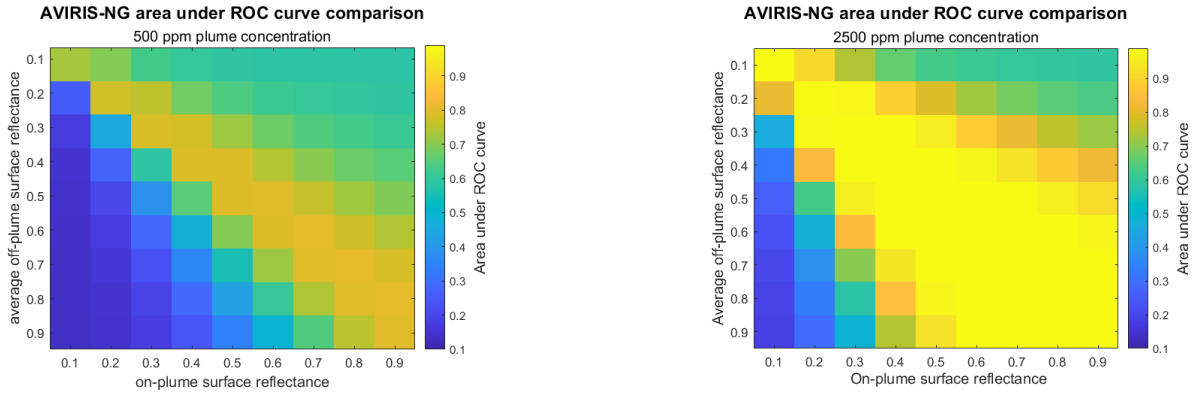

(a) (b)

Figure 5: AVIRIS-NG area under ROC curve heatmaps for (a) a 500 ppm plume and (b) a 2500 ppm plume

4.2 HyTES results

The factors with the highest impact on methane detectability for HyTES were the surface temperature, methane plume temperature, and methane concentration. In order to evaluate methane detectability at a variety of temperature conditions, we varied the surface and plume temperatures between 265-315 K, and repeated this for methane plumes with 500 ppm and 2500 ppm concentration. Figure 6 shows heatmaps of area under the ROC curve for these conditions. The surface temperature varies in the x direction and the plume temperature varies in the y direction. For both a 500 and 2500 ppm plume, the area under the ROC curve is close to 0.5 when plume temperature and surface temperature are equal. For a 500 ppm plume concentration, the methane plume was detectable with a temperature contrast of at least 12-15 K between plume and surface. A 2500 ppm concentration plume required only 2.5-4.0 K temperature contrast in order for methane to be detectable. For both 500 ppm and 2500 ppm methane plumes, the area under the ROC curve reached over 0.9 with sufficient temperature contrast, making both low and high concentration plumes highly detectable.

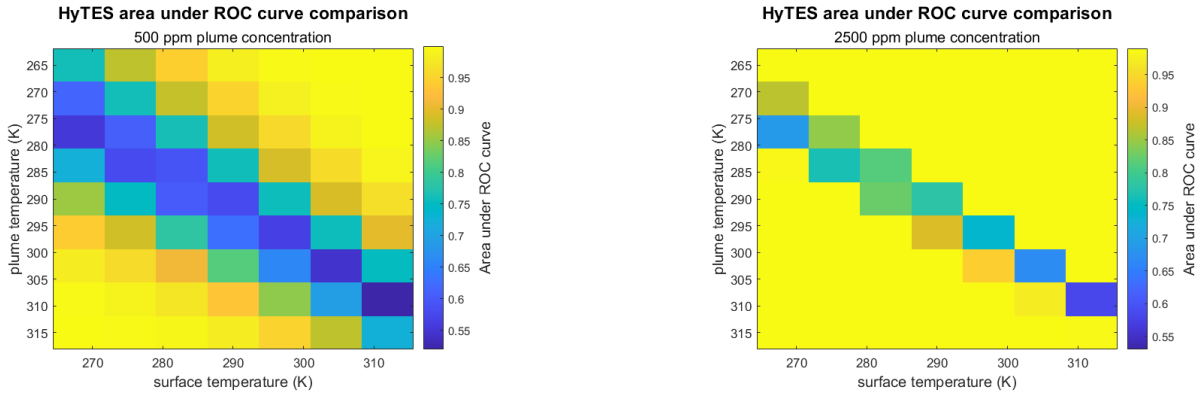

(a) (b)

Figure 6: HyTES results for (a) a 500 ppm plume and (b) a 2500 ppm plume

5. CONCLUSIONS AND FUTURE WORK

This study demonstrated that, in order to detect a methane plume, AVIRIS-NG required an on-plume to off-plume surface reflectance ratio in the range of 1.25-1.8 for low concentration plumes and 0.6-3.0 for high concentration plumes. HyTES required a temperature contrast between the plume and the surface of 12-15 K for a low concentration plume and 2.5-4.0 K for a high concentration plume. These trends indicate that HyTES may be more effective at detecting lower concentration plumes. For the 500 ppm plume, the area under the ROC curve for HyTES had a maximum of 0.99 with sufficient temperature contrast. For AVIRIS-NG however, even when the average on- and off-plume reflectances were within the detectable range, the area under the ROC curve did not surpass 0.85. For higher concentration plumes, AVIRIS-NG could detect methane for on- to off-plume reflectance ratios of 0.6-3.0, which encompasses a very broad range of possible conditions in a real scene. Even for higher concentration plumes, HyTES was still unable to detect a plume if it was at the same temperature as the surface. Based on these results, AVIRIS-NG could be a better detector for high concentration plumes, making it suited to detection of high concentration point sources. HyTES, because of its capability to detect lower concentration plumes, could be used for mapping methane plume distributions in areas where the plume has diffused into the ambient air and lowered in concentration, provided the ambient air temperature differs from the ground surface temperature.

This method of synthetic image generation and methane detection is applicable to other types of sensors; future work on this topic would include applying this method to other sensors in order to make broader generalizations about the tradeoffs of using the SWIR and the LWIR for methane detection.

REFERENCES

[1] Canadell, J., Monteiro, P., Costa, M., da Cunha, L. C., Cox, P., Eliseev, A., S. Henson, M. I., Jaccard, S., Koven, C., Lohila, A., P.K. Patra, a. S. P., Rogelj, J., Syampungani, S., Zaehle, S., and Zickfeld, K., [*Climate Change 2021: The Physical Science Basis. Contribution of Working Group I to the Sixth Assessment Report of the Intergovernmental Panel on Climate Change*], Cambridge University Press.

[2] Miller, S. M., Wofsy, S. C., Michalak, A. M., Kort, E. A., Andrews, A. E., Biraud, S. C., Dlugokencky, E. J., et al., "Anthropogenic emissions of methane in the united states," *Proceedings of the National Academy of Sciences* **110**(50), 20018–20022 (2013).

[3] Karakurt, I., Aydin, G., and Aydine., K., "Sources and mitigation of methane emissions by sectors: A critical review," *Renewable Energy* **39**, 40–48 (2012).

[4] Thorpe, A. K., Frankenberg, C., Thompson, D. R., Duren, R. M., Aubrey, A. D., Bue, B. D., Green, R. O., et al., "Airborne doas retrievals of methane, carbon dioxide, and water vapor concentrations at high spatial resolution: application to aviris-ng," *Atmospheric Measurement Techniques* **10**(10), 3833–3850 (2017).

[5] Duren, R. M., Thorpe, A. K., Foster, K. T., Rafiq, T., Hopkins, F. M., Yadav, V., Bue, B. D., et al., "California's methane super-emitters," *Nature* **575**(7781), 180–184 (2019).

[6] Hulley, G. C., Duren, R. M., Hopkins, F. M., Hook, S. J., Vance, N., Guillevic, P., Johnson, W. R., et al., "High spatial resolution imaging of methane and other trace gases with the airborne hyperspectral thermal emission spectrometer (hytes)," *Atmospheric Measurement Techniques* **9**(5), 2393–2408 (2016).

[7] Kuai, L., Worden, J. R., Li, K.-F., Hulley, G. C., Hopkins, F. M., Miller, C. E., Hook, S. J., Duren, R. M., and Aubrey., A. D., "Characterization of anthropogenic methane plumes with the hyperspectral thermal emission spectrometer (hytes): A retrieval method and error analysis," *Atmospheric Measurement Techniques* **9**(7), 3165–3173 (2016).

[8] Ayasse, A. K., Thorpe, A. K., Roberts, D. A., Funk, C. C., Dennison, P. E., Frankenberg, C., Steffke, A., and Aubrey, A. D., "Evaluating the effects of surface properties on methane retrievals using a synthetic airborne visible/infrared imaging spectrometer next generation (aviris-ng) image," *Remote sensing of environment* **215**, 386–397 (2018).

[9] Webber, C., *An Examination of Environmental Applications for Uncooled Thermal Infrared Remote Sensing Instruments.*, PhD thesis, Rochester Institute of Technology (2021).

[10] Berk, A., Conforti, P., Kennett, R., Perkins, T., Hawes, F., and Bosch., J. V. D., "Modtran 6: A major upgrade of the modtran® radiative transfer code," *2014 6th Workshop on Hyperspectral Image and Signal Processing: Evolution in Remote Sensing (WHISPERS)* (2014).

[11] Frankenberg, C., Thorpe, A. K., Thompson, D. R., Hulley, G., Kort, E. A., Vance, N., Borchardt, J., et al., "Airborne methane remote measurements reveal heavy-tail flux distribution in four corners region," *Proceedings of the national academy of sciences* **113**(35), 9743–9739 (2016).

[12] Chabrillat, S., Goetz, A. F., Krosley, L., and Olsen, H. W., "Use of hyperspectral images in the identification and mapping of expansive clay soils and the role of spatial resolution," *Remote sensing of Environment* **82**(2-3), 431–445 (2002).

[13] Cusworth, D. H., Jacob, D. J., Daniel J. Varon, a. C. C. M., Liu, X., Chance, K., Thorpe, A. K., et al., "Potential of next-generation imaging spectrometers to detect and quantify methane point sources from space," *Atmospheric Measurement Techniques* **12**(10), 5655–5668. (2019).

[14] Thompson, D. R., Thorpe, A. K., Frankenberg, C., Green, R. O., R. Duren, L. G., Hollstein, A., Middleton, E., Ong, L., and Ungar, S., "Space-based remote imaging spectroscopy of the aliso canyon ch4 superemitter," *Geophysical Research Letters* **43**(12), 6571–6578 (2016).

[15] Hook, S. and Team, T. H., "First flight of the hyperspectral thermal emission spectrometer (hytes) airborne instrument," Presented at: 2012 HyspIRI Workshop, Washington, DC USA. (2012).

[16] Dennison, P. E., Thorpe, A. K., Pardyjak, E. R., Roberts, D. A., Qi, Y., Green, R. O., Bradley, E. S., and Funk., C. C., "High spatial resolution mapping of elevated atmospheric carbon dioxide using airborne imaging spectroscopy: Radiative transfer modeling and power plant plume detection," *Remote sensing of environment* **139**, 116–129 (2013).

[17] Gordon, I., Rothman, L., Hill, C., Kochanov, R., Tan, Y., Bernath, P., Birk, M., Boudan, V., et al., "The hitran2016 molecular spectroscopic database," *Journal of Quantitative Spectroscopy and Radiative Transfer* **248**, 3–69 (2017).